



PCCP

**Tuning the odd–even effect on two-dimensional assemblies
of curcumin derivatives by alkyl chain substitution: A
scanning tunnelling microscopy study**

Journal:	<i>Physical Chemistry Chemical Physics</i>
Manuscript ID	CP-ART-01-2023-000368.R1
Article Type:	Paper
Date Submitted by the Author:	02-Mar-2023
Complete List of Authors:	Liu, Suyi; University of Tsukuba Faculty of Pure and Applied Sciences, Graduate School of Science and Technology; National Institute of Advanced Industrial Science and Technology Tsukuba Center Tsukuba Central Norikane, Yasuo; National Institute of Advanced Industrial Science and Technology Tsukuba Center Tsukuba Central, Tsuzuki, Seiji; The University of Tokyo, Applied Physics; Yokohama National University, Institute of Advanced Sciences Ito, Shotaro; National Institute of Advanced Industrial Science and Technology, Research Institute for Sustainable Chemistry Kikkawa, Yoshihiro; National Institute of Advanced Industrial Science and Technology (AIST),

SCHOLARONE™
Manuscripts

ARTICLE

Tuning the odd–even effect on two-dimensional assemblies of curcumin derivatives by alkyl chain substitution: A scanning tunnelling microscopy study

Received 00th January 20xx,
Accepted 00th January 20xx

DOI: 10.1039/x0xx00000x

Suyi Liu,^{a, b} Yasuo Norikane,^{*b, c} Seiji Tsuzuki,^d Shotaro Ito^e and Yoshihiro Kikkawa^{*b}

Well-ordered molecular arrangement on surfaces is fundamental for fabrications of functional molecular devices which are of particular interest in nanotechnology. In addition to nano-manufacturing, the production of useful materials from natural resources has recently attracted increasing attention. Herein, we focused on the two-dimensional (2D) self-assemblies of curcumin derivatives. The effects of the number, length, and substitution of the alkyl chains on the 2D structures of curcumin derivatives were studied by scanning tunnelling microscopy at the highly oriented pyrolytic graphite/1,2,4-trichlorobenzene interface. Curcumin derivatives containing both methoxy and alkoxy chain groups and those possessing four alkoxy chains exhibit linear structures with and without interdigitation of alkoxy chains, respectively. These 2D structure formations are independent of the alkyl chain length. However, the bisdemethoxycurcumin derivatives periodically form stair-like and linear structures depending on the alkyl chain length, which indicates the existence of the odd–even effect. These results suggest that the 2D structural modulation of curcumin derivatives caused by the odd–even effect can be tuned by the number of alkyl chain substituents. The appearance and disappearance of the odd–even effect in curcumin derivatives is discussed in terms of the balance between intermolecular and molecule–substrate interactions.

Introduction

Fine tuning of supramolecular structures on surfaces is essential for the fabrication of functional nanomaterials and molecular machines.¹ By introducing noncovalent interactions such as dispersion forces,² metal coordination,³ hydrogen bonding,⁴ and halogen bonding,⁵ various types of fascinating supramolecular structures have been constructed. Scanning tunnelling microscopy (STM) has been used for the direct visualization of two-dimensional (2D) molecular arrangements on surfaces.⁶

Modification of molecular structures that contain alkyl chain substituents significantly affects their intermolecular and molecule–substrate interactions, particularly on the highly oriented pyrolytic graphite (HOPG). The number, length, and substitution of the alkyl chains influence the 2D self-assemblies, and various types of molecular networks that are formed owing to these factors have been reported.⁷

The odd–even effect is a well-known phenomenon introduced by odd or even numbers of carbon atoms in the alkyl

chains, which causes alternative changes in the physical and chemical properties.^{7a, 8} For 2D and 3D systems, the odd–even effect has been discussed in terms of the direction of terminal methyl groups in the alkyl chains.^{8c} Although many studies related to the odd–even effect in 2D structures have been reported,⁹ the precise control of 2D structures based on the odd–even effect remains challenging.

In recent years, bio-based materials have attracted considerable attention both in scientific and industrial applications due to their eco-friendly characteristics.¹⁰ The 2D self-assembly of bio-based materials can be applied for fabricating functional nano-templates.¹¹ Curcumin, a natural polyphenol extracted from *Curcuma longa*, has been investigated in biomedical fields because of its anti-tumour activity, anti-Alzheimer's disease, and selective cytotoxicity.¹² To the best of our knowledge, the 2D self-assembly of curcumin derivatives on substrate surfaces has not been investigated so far.

In this study, we investigated the 2D self-assemblies of curcumin derivatives by STM at the HOPG / 1,2,4-trichlorobenzene (TCB) interface. The following differently substituted curcumin derivatives were prepared (Scheme 1): curcumin (**CR**) with two alkoxy chains in addition to the original methoxy groups, bisdemethoxycurcumin (**BC**), which contains two alkoxy chains, and tetra alkoxyated curcumin (**TC**). The alkyl chain lengths were changed from C15 to C18. Thus, the effects of the number of alkyl chains substituents and lengths on the 2D structures were investigated.

^a Graduate School of Science and Technology, University of Tsukuba, Ibaraki 305-8571, Japan

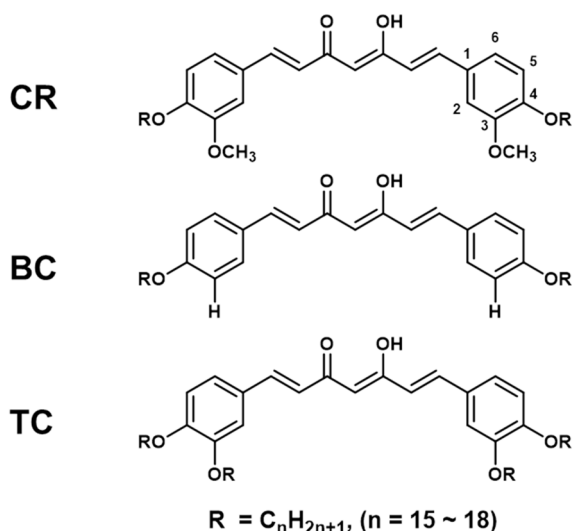
^b National Institute of Advanced Industrial Science and Technology (AIST), Tsukuba Central 5, 1-1-1 Higashi, Tsukuba, Ibaraki 305-8562, Japan
Email: y-norikane@aist.go.jp, y.kikkawa@aist.go.jp

^c Faculty of Pure and Applied Sciences, University of Tsukuba, Ibaraki 305-8571, Japan

^d Department of Applied Physics, The university of Tokyo, Tokyo 113-8656, Japan

^e National Institute of Advanced Industrial Science and Technology (AIST Chugoku), 3-11-32, Kagamiyama, Higashihiroshima, Hiroshima 739-0046, Japan

Electronic Supplementary Information (ESI) available: Additional STM images. See DOI: 10.1039/x0xx00000x



Scheme 1 Chemical structure of curcumin derivatives

Experimental section

All chemicals were purchased from either Kanto Chemicals, Kishida Chemicals, or Tokyo Chemical Industry and were used without further purification. The prepared compounds were characterized by ^1H and ^{13}C NMR spectroscopy (Bruker Avance 400 NMR spectrometer) with tetramethylsilane as the internal standard. Matrix-assisted laser desorption ionization time-of-flight mass spectrometry (MALDI-TOF MS) measurements were performed on a JEOL JMS-S3000 spectrometer with *trans*-2-[3-4-*tert*-butylphenyl]-2-methyl-2-propenylidene]malonitrile (DCTB) as the matrix.

Synthesis of CR compounds

Curcumin (1 mmol) and K_2CO_3 (6 mmol) were added in dry acetone (20 mL). The solution was stirred at 58 °C for 30 min. Subsequently, 1-Bromoalkane (3 mmol) was added into the solution, and the resultant solution was refluxed overnight with stirring. After removing the solvent *in vacuo*, 1 N hydrochloric acid was added to it to adjust the pH to 5, and the product was extracted with $\text{CHCl}_3/\text{H}_2\text{O}$, dried with anhydrous MgSO_4 , and filtered. After the evaporation of CHCl_3 , the crude product was purified by silica gel column chromatography using CHCl_3 /hexane (1:1) as the eluent. The CR compounds were obtained as yellow solids.

CR15: ^1H NMR (400 MHz, CDCl_3 , Me_4Si): δ 0.88 (6H, t, $J = 6.6$ Hz), 1.26 (44H, m), 1.46 (4H, m), 1.86 (4H, m), 3.91 (6H, s), 4.05 (4H, t, $J = 6.9$ Hz), 5.81 (1H, s), 6.49 (2H, d, $J = 15.7$ Hz), 6.87 (2H, d, $J = 8.4$ Hz), 7.09 (4H, m) and 7.60 (2H, d, $J = 15.7$ Hz). ^{13}C NMR (CDCl_3): δ 14.15, 22.71, 25.95, 29.06, 29.39, 29.41, 29.57, 29.62, 29.68, 29.71, 31.94, 55.99, 69.01, 76.76, 77.07, 77.39, 101.28, 110.22, 112.36, 121.85, 122.63, 127.83, 140.45, 149.50, 150.72, 183.26. Yield: 53 %. IR (KBr): 2998, 2919, 2850, 1631, 1583, 1510, 1421, 1261, 1031, 964, 844 cm^{-1} . MALDI-TOF MS $[\text{M} + \text{Na}]^+$ calculated for $\text{C}_{51}\text{H}_{80}\text{O}_6\text{Na}$, 811.5847; found 811.5847.

CR16: ^1H NMR (400 MHz, CDCl_3 , Me_4Si): δ 0.88 (6H, t, $J = 6.6$ Hz), 1.26 (48H, m), 1.46 (4H, m), 1.86 (4H, m), 3.91 (6H, s), 4.05 (4H, t, $J = 6.9$ Hz), 5.81 (1H, s), 6.49 (2H, d, $J = 15.7$ Hz), 6.87 (2H, d, $J = 8.4$ Hz), 7.09 (4H, m) and 7.60 (2H, d, $J = 15.7$ Hz). ^{13}C NMR (CDCl_3): δ 14.14, 22.70, 25.94, 29.05, 29.38, 29.45, 29.56, 29.60, 29.67, 29.71, 31.94, 56.01, 69.03, 76.73, 77.05, 77.36, 101.25, 110.21, 112.38, 121.85, 122.64, 127.84, 140.47, 149.51, 150.73, 183.26. Yield: 51 %. IR (KBr): 2998, 2919, 2850, 1631, 1583, 1510, 1421, 1261, 1031, 964, 844 cm^{-1} . MALDI-TOF MS $[\text{M} + \text{Na}]^+$ calculated for $\text{C}_{53}\text{H}_{84}\text{O}_6\text{Na}$, 839.6160; found 8339.6175.

CR17: ^1H NMR (400 MHz, CDCl_3 , Me_4Si): δ 0.88 (6H, t, $J = 6.6$ Hz), 1.26 (52H, m), 1.46 (4H, m), 1.86 (4H, m), 3.91 (6H, s), 4.05 (4H, t, $J = 6.9$ Hz), 5.81 (1H, s), 6.49 (2H, d, $J = 15.7$ Hz), 6.87 (2H, d, $J = 8.4$ Hz), 7.09 (4H, m) and 7.60 (2H, d, $J = 15.7$ Hz). ^{13}C NMR (CDCl_3): δ 14.13, 22.70, 25.93, 29.04, 29.37, 29.55, 29.60, 29.66, 29.70, 31.93, 56.01, 69.03, 76.71, 77.03, 77.34, 101.24, 110.20, 112.38, 121.85, 122.63, 127.83, 140.46, 149.51, 150.72, 183.26. Yield: 50 %. IR (KBr): 2998, 2921, 2850, 1631, 1583, 1510, 1421, 1263, 1031, 964, 844 cm^{-1} . MALDI-TOF MS $[\text{M} + \text{Na}]^+$ calculated for $\text{C}_{55}\text{H}_{88}\text{O}_6\text{Na}$, 867.6473; found 867.6455.

CR18: ^1H NMR (400 MHz, CDCl_3 , Me_4Si): δ 0.88 (6H, t, $J = 6.6$ Hz), 1.26 (56H, m), 1.46 (4H, m), 1.86 (4H, m), 3.91 (6H, s), 4.05 (4H, t, $J = 6.9$ Hz), 5.81 (1H, s), 6.49 (2H, d, $J = 15.7$ Hz), 6.87 (2H, d, $J = 8.4$ Hz), 7.09 (4H, m) and 7.60 (2H, d, $J = 15.7$ Hz). ^{13}C NMR (CDCl_3): δ 14.14, 22.70, 25.94, 29.05, 29.38, 29.56, 29.60, 29.67, 29.72, 31.94, 56.01, 69.03, 76.72, 77.04, 77.36, 101.25, 110.26, 112.38, 121.86, 122.94, 127.84, 140.47, 149.51, 150.73, 183.26. Yield: 56 %. IR (KBr): 2998, 2920, 2848, 1631, 1538, 1511, 1421, 1263, 1032, 964, 844 cm^{-1} . MALDI-TOF MS $[\text{M} + \text{Na}]^+$ calculated for $\text{C}_{57}\text{H}_{92}\text{O}_6\text{Na}$, 895.6786; found 895.6815.

Synthesis of BC compounds

The preparation of BC compounds was similar to that of the CR compounds; however, curcumin was replaced by bisdemethoxycurcumin in this procedure.

BC15: ^1H NMR (400 MHz, CDCl_3 , Me_4Si): δ 0.88 (6H, t, $J = 5.8$ Hz), 1.26 (44H, m), 1.46 (4H, m), 1.79 (4H, m), 3.99 (4H, t, $J = 6.5$ Hz), 5.78 (1H, s), 6.49 (2H, d, $J = 15.8$ Hz), 6.90 (4H, d, $J = 8.8$ Hz), 7.49 (4H, d, $J = 8.8$ Hz) and 7.62 (2H, d, $J = 15.8$ Hz). ^{13}C NMR (CDCl_3): δ 14.14, 22.72, 26.02, 29.19, 29.39, 29.61, 29.70, 31.95, 68.21, 101.34, 114.91, 121.66, 127.58, 129.78, 140.22, 160.95, 183.39. IR (KBr): 2954, 2917, 2848, 1644, 1510, 1421, 1265, 1110, 1032, 962, 840 cm^{-1} . Yield: 51 %. MALDI-TOF MS $[\text{M} + \text{Na}]^+$ calculated for $\text{C}_{49}\text{H}_{76}\text{O}_4\text{Na}$, 751.5636; found 751.5606.

BC16: ^1H NMR (400 MHz, CDCl_3 , Me_4Si): δ 0.88 (6H, t, $J = 5.8$ Hz), 1.26 (48H, m), 1.46 (4H, m), 1.79 (4H, m), 3.99 (4H, t, $J = 6.5$ Hz), 5.78 (1H, s), 6.49 (2H, d, $J = 15.7$ Hz), 6.90 (4H, d, $J = 8.8$ Hz), 7.49 (4H, d, $J = 8.8$ Hz) and 7.62 (2H, d, $J = 15.8$ Hz). ^{13}C NMR (CDCl_3): δ 14.13, 22.71, 26.01, 29.17, 29.19, 29.39, 29.70, 31.96, 68.18, 101.36, 114.90, 121.64, 127.56, 129.79, 140.23, 160.93, 183.38. IR (KBr): 2953, 2917, 2848, 1643, 1510, 1421, 1263, 1110, 1032, 962, 840 cm^{-1} . Yield: 53 %.

MALDI-TOF MS $[M + Na]^+$ calculated for $C_{51}H_{80}O_4Na$, 779.5949; found 779.5919.

BC17: 1H NMR (400 MHz, $CDCl_3$, Me_4Si): δ 0.88 (6H, t, $J = 6.8$ Hz), 1.26 (52H, m), 1.46 (4H, m), 1.79 (4H, m), 3.99 (4H, t, $J = 6.5$ Hz), 5.78 (1H, s), 6.49 (2H, d, $J = 15.8$ Hz), 6.90 (4H, d, $J = 8.7$ Hz), 7.49 (4H, d, $J = 8.8$ Hz) and 7.62 (2H, d, $J = 15.8$ Hz). ^{13}C NMR ($CDCl_3$): δ 14.13, 22.70, 26.00, 29.17, 29.37, 29.59, 29.70, 31.93, 68.18, 101.32, 114.90, 121.64, 127.58, 129.76, 140.20, 160.91, 183.37. IR (KBr): 2954, 2917, 2848, 1644, 1511, 1421, 1265, 1110, 1032, 962, 840 cm^{-1} . Yield: 52 %. MALDI-TOF MS $[M + Na]^+$ calculated for $C_{53}H_{84}O_4Na$, 807.6262, found 807.6247.

BC18: 1H NMR (400 MHz, $CDCl_3$, Me_4Si): δ 0.88 (6H, t, $J = 5.8$ Hz), 1.26 (56H, m), 1.46 (4H, m), 1.79 (4H, m), 3.99 (4H, t, $J = 6.6$ Hz), 5.78 (1H, s), 6.49 (2H, d, $J = 15.8$ Hz), 6.90 (4H, d, $J = 8.8$ Hz), 7.49 (4H, d, $J = 8.8$ Hz) and 7.62 (2H, d, $J = 15.8$ Hz). ^{13}C NMR ($CDCl_3$): δ 14.13, 22.70, 26.00, 29.17, 29.37, 29.59, 29.70, 31.93, 68.18, 101.32, 114.90, 121.64, 127.58, 129.76, 140.20, 160.91, 183.37. IR (KBr): 2954, 2917, 2848, 1643, 1538, 1511, 1421, 1265, 1022, 962, 840 cm^{-1} . Yield: 53 %. MALDI-TOF MS $[M + Na]^+$ calculated for $C_{55}H_{88}O_4Na$, 835.6575; found 835.6546.

Synthesis of TC compounds

TC compounds were synthesized by the aldol condensation of 3,4-dialkyloxybenzaldehydes with acetylacetone and butylamine.¹³ 3,4-dialkyloxybenzaldehydes with different alkyl chain lengths were prepared from 3,4-dihydroxybenzaldehyde (1 mmol) and 1-bromoalkane (2 mmol). Subsequently, boron trioxide (1 mmol) and acetylacetone (2 mmol) were added in ethyl acetate at 70 °C for 3h, and the precipitate was filtered and washed with hexane. The residue was added in ethyl acetate with 3,4-dialkyloxybenzaldehydes (4 mmol) and tributyl borate (4 mmol), and the resultant solution was stirred for 1 h at 70 °C. Then, *n*-butylamine (0.2 mmol) dissolved in ethyl acetate was added to this mixture dropwise, which was stirred overnight. Finally, 1 N hydrochloric acid was added to this solution to adjust the pH to 5. The solution was stirred for 1 h at 60 °C to quench the reaction. Then, the solvent was removed in *vacuo*, and the product was extracted with $CHCl_3/H_2O$, dried with anhydrous $MgSO_4$ and filtered. The crude product was purified by silica gel column chromatography using $CHCl_3$ /hexane (1:1) as the eluent to afford the **TC** compounds as orange solids.

TC15: 1H NMR (400 MHz, $CDCl_3$, Me_4Si): δ 0.88 (12H, t, $J = 7.0$ Hz), 1.26 (88H, m), 1.47 (4H, m), 1.56 (4H, s), 1.83 (8H, m), 4.02 (8H, t, $J = 6.6$ Hz), 5.80 (1H, s), 6.47 (2H, d, $J = 15.7$ Hz), 6.86 (2H, d, $J = 8.2$ Hz), 7.09 (4H, m) and 7.58 (2H, d, $J = 15.8$ Hz). ^{13}C NMR ($CDCl_3$): δ 14.14, 22.72, 26.02, 26.06, 28.93, 29.16, 29.28, 29.39, 29.41, 29.46, 29.65, 29.69, 29.74, 31.95, 69.10, 69.38, 101.21, 112.45, 113.06, 121.81, 122.68, 127.94, 140.54, 149.20, 151.34, 183.30. IR (KBr): 2954, 2917, 2850, 1627, 1581, 1419, 1255, 1172, 1135, 1072, 1010, 973, 844 cm^{-1} . Yield: 15 %. MALDI-TOF MS $[M + Na]^+$ calculated for $C_{79}H_{136}O_6Na$, 1204.0229; found 1204.0259.

TC16: 1H NMR (400 MHz, $CDCl_3$, Me_4Si): δ 0.88 (12H, t, $J = 7.0$ Hz),

1.26 (96H, m), 1.47 (4H, m), 1.56 (4H, s), 1.83 (8H, m), 4.02 (8H, t, $J = 6.6$ Hz), 5.80 (1H, s), 6.47 (2H, d, $J = 15.7$ Hz), 6.86 (2H, d, $J = 8.2$ Hz), 7.09 (4H, m) and 7.58 (2H, d, $J = 15.8$ Hz). ^{13}C NMR ($CDCl_3$): δ 14.14, 22.71, 26.02, 26.06, 28.93, 29.16, 29.28, 29.39, 29.41, 29.46, 29.64, 29.69, 29.74, 31.95, 69.10, 69.39, 101.21, 112.46, 113.06, 121.81, 122.68, 127.94, 140.54, 149.21, 151.34, 183.30. IR (KBr): 2954, 2917, 2850, 1627, 1583, 1419, 1257, 1172, 1136, 1068, 1010, 973, 844 cm^{-1} . Yield: 22 %. MALDI-TOF MS $[M + Na]^+$ calculated for $C_{83}H_{144}O_6Na$, 1260.0851; found 1260.0880.

TC17: 1H NMR (400 MHz, $CDCl_3$, Me_4Si): δ 0.88 (12H, t, $J = 7.0$ Hz), 1.26 (104H, m), 1.47 (4H, m), 1.56 (4H, s), 1.83 (8H, m), 4.02 (8H, t, $J = 6.6$ Hz), 5.80 (1H, s), 6.47 (2H, d, $J = 15.7$ Hz), 6.86 (2H, d, $J = 8.2$ Hz), 7.09 (4H, m) and 7.58 (2H, d, $J = 15.8$ Hz). ^{13}C NMR ($CDCl_3$): δ 14.14, 22.71, 26.02, 26.06, 28.94, 29.16, 29.28, 29.39, 29.41, 29.46, 29.65, 29.69, 29.74, 31.95, 69.10, 69.38, 101.21, 112.46, 113.06, 121.81, 122.68, 127.94, 140.54, 149.21, 151.34, 183.30. IR (KBr): 2954, 2917, 2850, 1627, 1583, 1419, 1257, 1172, 1137, 1068, 1010, 973, 840 cm^{-1} . Yield: 18 %. MALDI-TOF MS $[M + Na]^+$ calculated for $C_{87}H_{152}O_6Na$, 1316.1481; found 1316.1485.

TC18: 1H NMR (400 MHz, $CDCl_3$, Me_4Si): δ 0.88 (12H, t, $J = 7.0$ Hz), 1.26 (112H, m), 1.47 (4H, m), 1.56 (4H, s), 1.83 (8H, m), 4.02 (8H, t, $J = 6.6$ Hz), 5.80 (1H, s), 6.47 (2H, d, $J = 15.7$ Hz), 6.86 (2H, d, $J = 8.2$ Hz), 7.09 (4H, m) and 7.58 (2H, d, $J = 15.8$ Hz). ^{13}C NMR ($CDCl_3$): δ 14.13, 22.70, 26.02, 26.06, 28.93, 29.16, 29.28, 29.38, 29.41, 29.45, 29.64, 29.68, 29.73, 31.94, 69.10, 69.39, 101.20, 112.48, 113.07, 121.82, 122.67, 127.95, 140.53, 149.21, 151.35, 183.29. IR (KBr): 2954, 2916, 2850, 1627, 1583, 1419, 1257, 1170, 1134, 1066, 1010, 973, 846 cm^{-1} . Yield: 25 %. MALDI-TOF MS $[M + Na]^+$ calculated for $C_{91}H_{160}O_6Na$, 1372.2107; found 1372.2078.

STM observations

The prepared **CR**, **BC**, and **TC** compounds were dissolved in TCB at the concentration of 0.1 mM. The TCB solutions were deposited on the freshly cleaved HOPG surface, and a cut Pt/Ir wire (90/10; 0.25 mm ϕ) was used as the STM tip. STM images were acquired at the HOPG/TCB interface by Nanoscope IIIa STM (Digital Instruments). The SPIP software (Image Metrology) was applied to calibrate and correct the STM images based on the HOPG lattice underneath the monolayer.

DFT calculations

The Gaussian 16 program¹⁴ was used for DFT calculations. The geometry optimisation was carried out at the B3LYP/6-31G* level¹⁵ with Grimme's D3 dispersion correction.¹⁶ The adsorption energy (E_{ad}) was calculated as the sum of the interaction energy (E_{int}) and the deformation energy of the adsorbed molecule (E_{def}). The E_{int} was calculated at the B3LYP/6-311G** level with Grimme's D3 dispersion correction. The BSSE was corrected by the counterpoise method.¹⁷ The E_{def} represents the increase in the energy of the adsorbed molecule owing to the deformation associated with the adsorption.

The E_{def} was calculated at the B3LYP/6-311G** level with Grimme's D3 dispersion correction.

Result and discussion

Self-assembly of CR compounds

The STM images and 2D structures of CR compounds with different alkyl chain lengths are shown in Figs. 1 and S1. The STM images contain bright and dark regions. The bright regions are considered as the curcumin cores because of the high tunnelling current of their π -conjugated backbones. The dark regions contain long alkyl chains aligned along one of the symmetric axes of the HOPG lattice directions indicated by white arrows. In Fig. 1A, CR15 exhibits a columnar structure, in which the molecules in adjacent columns are directed towards opposite directions possibly due to their polarities. The distance between two curcumin cores was measured to be 0.9 ± 0.1 nm, which corresponds to the lattice constants along the a -axis (Table 1). This value is almost twice the reported equilibrium distance between two n -alkanes ($0.46 \text{ nm} \times 2$).¹⁸ The distance between the two dark regions L_1 was measured as 2.1 ± 0.1 nm, which is almost identical to the calculated length of the pentadecyloxy chain (1.9 nm). These results indicate that the alkyl chains are interdigitated. Based on these results, the proposed molecular models were overlapped on the STM image. The lattice constants of the CR molecules are listed in Table 1.

In Figs. 1B-D, CR16, CR17, and CR18 also exhibited the columnar structures. The distance between two adjacent curcumin cores was approximately 1 nm (lattice constants along a -axis listed in Table 1). In addition, the lengths of dark regions, namely $L_2 = 2.2 \pm 0.1$ nm, $L_3 = 2.2 \pm 0.1$ nm, and $L_4 = 2.3 \pm 0.1$ nm,

were almost identical to the calculated chain lengths of 2.02 nm, 2.15 nm and 2.27 nm, respectively. These results suggest that the alkyl chains of the CR compounds are all interdigitated. Thus, CR compounds formed similar linear structures, regardless of the alkyl chain length.

Table 1 Lattice constants and unit cell parameters of CR compounds measured from the STM images.

Molecule	a (nm)	b (nm)	γ (deg)	N^a	D^b (nm ⁻²)
CR15	0.93 ± 0.08	3.96 ± 0.07	82 ± 1	1	0.27
CR16	0.93 ± 0.04	4.20 ± 0.10	84 ± 2	1	0.26
CR17	0.95 ± 0.03	4.36 ± 0.07	84 ± 2	1	0.24
CR18	0.94 ± 0.04	4.59 ± 0.04	84 ± 2	1	0.23

^a N = the number of molecules per unit cell. ^b D (molecular density) = N divided by unit cell area.

Self-assembly of BC compounds

To investigate the effect of methoxy groups on the 2D molecular arrangements of curcumin derivatives, the STM images of BC compounds were obtained. As shown in Figs. 2A and S2A, BC15 compounds form clusters containing five BC15 cores, which are depicted by the red rectangles in the STM images. These cores were arranged into a stair-like structure. In these clusters, the distance between the two neighbouring cores is 0.9 ± 0.1 nm, suggesting that the alkyl chains are interdigitated. This observation was similar to the case of the CR compounds. Two molecules from the ends of the

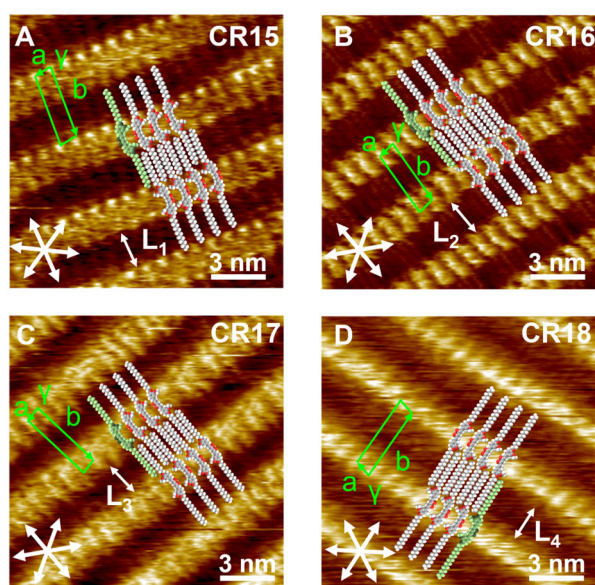


Fig. 1 STM images of CR compounds ($n = 15-18$) physisorbed at the HOPG/TCB interface and the proposed molecular models based on the STM images. One of the molecular constituents is coloured in green. The sets of white arrows in each figure indicate the HOPG lattice directions. The distances between dark regions: $L_1 = 2.0 \pm 0.1$ nm, $L_2 = 2.1 \pm 0.1$ nm, $L_3 = 2.2 \pm 0.1$ nm and $L_4 = 2.3 \pm 0.1$ nm. Tunnelling conditions: (A) $I = 30$ pA, $V = -1200$ mV; (B) $I = 30$ pA, $V = -390$ mV; (C) $I = 30$ pA, $V = -800$ mV; (D) $I = 30$ pA, $V = -850$ mV.

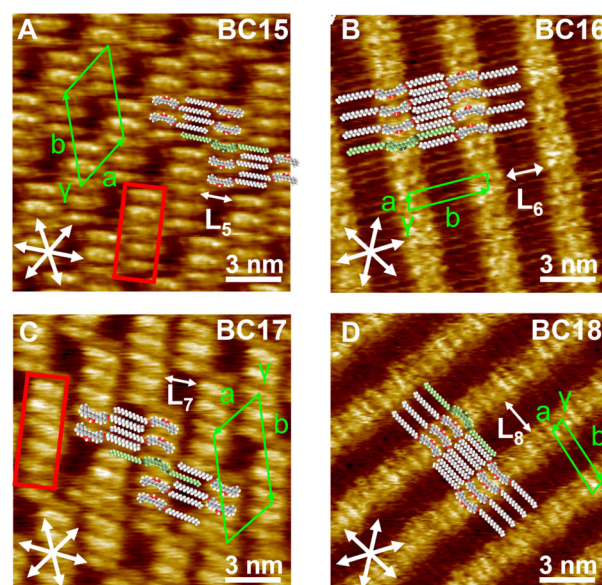


Fig. 2 STM images of BC compounds ($n = 15-18$) physisorbed at the HOPG/TCB interface and the proposed molecular models based on the STM images. One of the molecular constituents is coloured in green. The sets of white arrows in each figure indicate the HOPG lattice directions. The distances between dark regions: $L_5 = 1.8 \pm 0.1$ nm, $L_6 = 1.9 \pm 0.1$ nm, $L_7 = 2.0 \pm 0.1$ nm and $L_8 = 2.1 \pm 0.1$ nm. Tunnelling conditions: (A) $I = 30$ pA, $V = -350$ mV; (B) $I = 30$ pA, $V = -1100$ mV; (C) $I = 30$ pA, $V = -900$ mV; (D) $I = 30$ pA, $V = -800$ mV.

clusters at one side were in close contact with the adjacent clusters, while the middle molecule was isolated. At the area of contact, there was no space to accommodate the alkyl chains, indicating that one of the alkyl chains of **BC15** dangled into the solvent phase.^{7b, d} In contrast, the alkyl chains of the isolated molecules were fully adsorbed on the HOPG surface. The length of the dark region of **BC15** was measured to be $L_5 = 1.8 \pm 0.1$ nm, which is almost identical to the calculated length of the pentadecyloxy chain (1.9 nm). According to these results, the proposed molecular models were overlapped on the STM images. The lattice constants of **BC15** are listed in Table 2. Figs. 2C and S2C shows the 2D structures of **BC17**, which showed similar molecular arrangements to that of **BC15**. Most clusters of **BC17** are composed of five molecules, as shown in Fig. S2C. However, some slips and defects exist in the 2D structures as indicated by blue arrows, resulting in some six-membered clusters.

Interestingly, **BC16** and **BC18** displayed columnar structures (Figs. 2B, 2D, S2B, and S2D), which were completely different from the stair-like structures of **BC15** and **BC17**. The distance between the **BC16** and **BC18** cores corresponding to the a -axis was almost twice the intermolecular distance between n -alkane dimers ($0.46 \text{ nm} \times 2$). This result suggests that the alkyl chains were interdigitated. The proposed molecular models were overlapped on the STM images. The lattice constants of **BC** molecules are listed in Table 2. These results suggest that the 2D structures are modulated based on the alkyl chain length, and the odd–even effect appears in the **BC** compounds.

Table 2 Lattice constants and unit cell parameters of **BC** compounds measured from the STM images.

Molecule	a (nm)	b (nm)	γ (deg)	N^a	D^b (nm ⁻²)
BC15	3.22 ± 0.05	5.55 ± 0.07	58 ± 2	5	0.33
BC16	0.91 ± 0.07	4.19 ± 0.10	76 ± 2	1	0.27
BC17	3.52 ± 0.02	5.62 ± 0.06	56 ± 1	5	0.30
BC18	0.95 ± 0.07	4.23 ± 0.05	87 ± 1	1	0.25

^a N = the number of molecules per unit cell. ^b D (molecular density) = N divided by unit cell area.

Self-assembly of TC compounds

To further examine the effect of alkoxy substituents at the 3-position, the STM images of **TC** compounds were obtained. Figs. 3A and S3A show the self-assembled structures of **TC15** molecules, which also exhibit columnar structures. However, the bright regions were obliquely oriented against the columnar axis. The distance between two adjacent **TC15** cores in a column was measured as 2.56 ± 0.07 nm (a -axis, Table 3), and that between the adjacent columns L_9 was measured as 1.9 ± 0.1 nm. These results suggest that there is enough space to accommodate all the alkyl chains with interdigitation. Moreover, vacant spaces were observed between the cores displayed as bright lines, which can be filled with the solvent of the TCB molecules.¹⁹ Therefore, TCB not only acts as a dispersant, but also as a filler in vacant spaces, which improves the

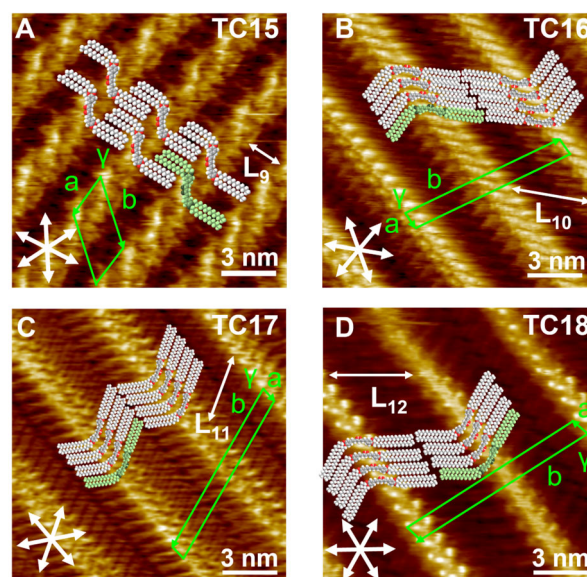


Fig. 3 STM images of **TC** compounds ($n = 15-18$) physisorbed at the HOPG/TCB interface and the proposed molecular models based on the STM images. One of the molecular constituents is coloured in green. The sets of white arrows in each figure indicate the HOPG lattice directions. The distances between dark regions: $L_9 = 1.9 \pm 0.1$ nm, $L_{10} = 4.0 \pm 0.2$ nm, $L_{11} = 4.2 \pm 0.2$ nm and $L_{12} = 4.5 \pm 0.1$ nm. Tunnelling conditions: (A) $I = 30$ pA, $V = -950$ mV; (B) $I = 30$ pA, $V = -900$ mV; (C) $I = 30$ pA, $V = -800$ mV; (D) $I = 30$ pA, $V = -850$ mV.

stability of the structure. The proposed molecular models are overlapped on STM images, and the molecules adopt a Z-like conformation.

The STM images and 2D structures of **TC16-18** are shown in Figs. 3B-D and S3B-D, respectively. The distance between the bright columns expanded, and the curcumin cores were aligned in the direction of one of the side chains. The lengths of the dark regions with straight-lined contrast were as follows: $L_{10} = 4.0 \pm 0.2$ nm, $L_{11} = 4.2 \pm 0.2$ nm, and $L_{12} = 4.5 \pm 0.1$ nm. These values are almost twice that of the corresponding alkyl chain lengths. In addition, the distance between adjacent the **TC16**, **TC17**, and **TC18** cores were 1.1 ± 0.1 nm, 1.0 ± 0.1 nm, and 1.0 ± 0.1 nm, respectively. These results suggest that the alkyl chains are no longer interdigitated but adopt a tail-to-tail arrangement with a V-shaped conformation. Notably, two different contacting modes of the alkyl chain terminals were observed, including the straight (α) and diagonal contacts (β), which

Table 3 Lattice constants and unit cell parameters of **TC** compounds measured from the STM images.

Molecule	a (nm)	b (nm)	γ (deg)	N^a	D^b (nm ⁻²)
TC15	2.56 ± 0.07	4.20 ± 0.04	53 ± 2	1	0.12
TC16	1.05 ± 0.05	11.7 ± 0.08	73 ± 2	2	0.17
TC17	1.07 ± 0.03	12.1 ± 0.14	73 ± 2	2	0.16
TC18	1.05 ± 0.03	12.4 ± 0.13	75 ± 2	2	0.16

^a N = the number of molecules per unit cell. ^b D (molecular density) = N divided by unit cell area.

were randomly observed in the **TC16-18** compounds (Fig. S3B-D). Based on these results, the proposed molecular models are overlapped on STM images. The lattice constants of the **TC** molecules are listed in Table 3.

Odd–even effect induced by alkyl chain substitution

In Figs. 1-3, the 2D structures of curcumin derivatives containing different alkyl substitutions and chain lengths (from C15 to C18) were revealed by STM at the HOPG/TCB interface. Their structural features are summarized in Fig. 4. **CR** and **TC** compounds showed columnar structures regardless of the alkyl chain length, whereas **BC** compounds periodically showed stair-like and linear structures depending on the alkyl chain length. These observations indicate that the absence of substituents at the 3-position affects the appearance of the odd–even effect.

To understand the mechanism of the appearance/disappearance of the odd–even effect, DFT calculations of 1-butoxy-2-methoxybenzene (**M4**) and butoxybenzene (**B4**) were carried out as simplified models of **CR** and **BC** compounds, respectively (Figs. 5A and 5D). The geometry optimisations of **M4** were started from two plausible orientations (types A and B) based on the stable geometries reported for *o*-dimethoxybenzene.²⁰ The two optimised geometries of **M4** are shown in Fig. 5B. In **M4-A**, the methoxy and butoxy groups are coplanar with the benzene ring and are oriented in opposite directions. In contrast, in **M4-B**, the butoxy group is coplanar to the benzene ring, and the methoxy group is 70° out of

	Substituent at 3-position	Alkyl carbon numbers				Odd-even effect
		15	16	17	18	
CR	✓	Linear	Linear	Linear	Linear	
BC		Stair-like	Linear	Stair-like	Linear	✓
TC	✓	Linear (Z-like)	Linear (V-like)	Linear (V-like)	Linear (V-like)	

Fig. 4 Summary of the 2D structural formation of curcumin derivatives observed by STM. Conformations of **TC** compounds are given in parentheses.

plane with respect to benzene. In the case of **B4**, the benzene ring and butoxy chain are coplanar. (Fig. 5E)

Next, the complex of **M4** with $C_{96}H_{24} was optimised as a model of adsorption for **M4** onto HOPG. The optimised geometry of the isolated $C_{96}H_{24}$ was used for the geometry optimisation of the complex. The geometry of $C_{96}H_{24}$ was fixed during the geometry optimisation. Fig. 5C shows the optimised geometries of the two types of **M4** adsorbed on $C_{96}H_{24}$. The adsorption energies (E_{ad}) calculated for **M4-A** and **M4-B** are -23.4 and -21.9 kcal/mol, respectively. This result indicates that the E_{ad} of **M4-A** is -1.5 kcal/mol larger (more negative) than that of **M4-B**. When **B4** is adsorbed on $C_{96}H_{24}$, it adopts a planar geometry (Fig. 5F). The E_{ad} calculated for **B4** is -20.2 kcal/mol. The E_{ad} for **M4-A** is -3.2 kcal/mol larger than that for **B4**, suggesting that the interactions of methoxy group of **M4-A** with $C_{96}H_{24}$ increase the adsorption energy.$

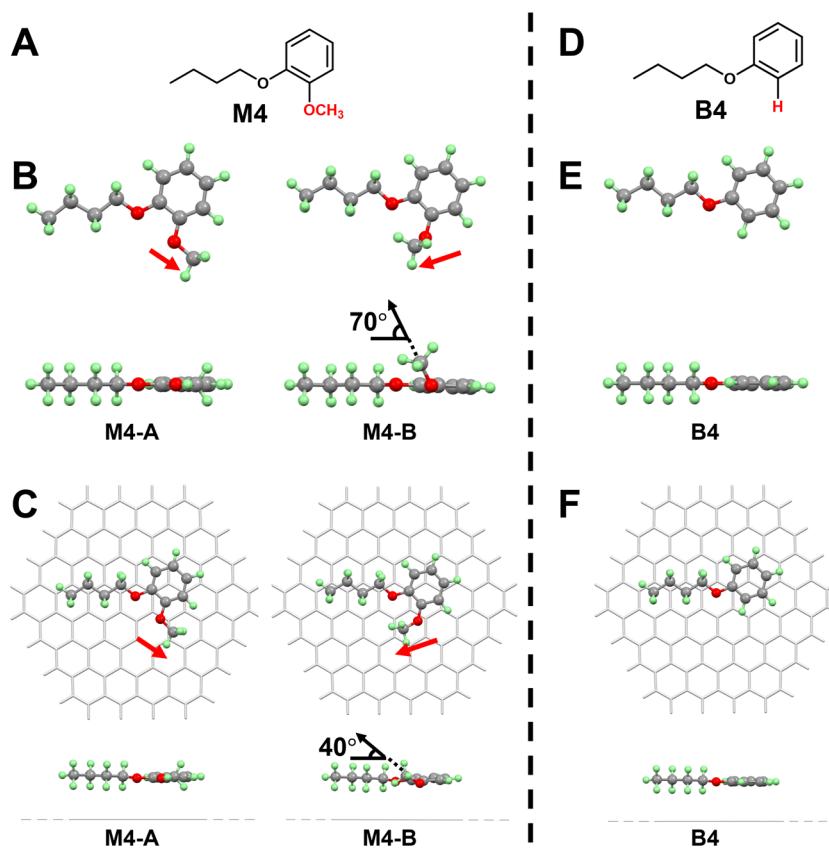


Fig. 5 Chemical structures **M4** (A) and **B4** (D). Optimised geometries of **M4** and **B4** in gas phase (B, E) and adsorbed on $C_{96}H_{24}$ (C, F) obtained from dispersion-corrected DFT calculation.

Since the **CR** compounds have two methoxy groups, the E_{ad} of **CR** is expected to be approximately 6 kcal/mol larger than that of corresponding the **BC** compounds, which have the same alkyl chain length. These results suggest that molecule–substrate (graphite) interaction is stronger in the self-assembly of the **CR** compounds than that in the corresponding **BC** compounds. The methoxy groups in the **CR** compounds help to firmly anchor the molecules on the HOPG surface, making the self-assemblies of **CR** compounds relatively insensitive to the intermolecular interactions among alkyl chain end groups. However, the self-assemblies of the **BC** compounds, which have weaker adsorption energies than the **CR** compounds, can be dominated by the intermolecular interactions among the adsorbed molecules. Therefore, the interaction among the terminal methyl groups in **BC** compounds enable the 2D structural modulation based on the odd–even effect. The number of carbon atoms in the alkyl chains of **TC** compounds is much larger than that in the **CR** compounds, indicating that the adsorption energies of **TC** compounds are significantly larger than those of the **CR** and **BC** compounds. Therefore, the self-assemblies of **TC** compounds are predominantly governed by molecule–substrate interactions, and the odd–even effect disappears.

Thus, we found that even simple modifications of chemical structures, such as methoxy group substitutions, severely affect the intermolecular interactions, especially molecule–substrate interactions. This result suggests that adjusting the balance of these interactions modulate the appearance/disappearance of the odd–even effect, enabling the 2D structural control of curcumin derivatives.

Conclusion

Curcumin derivatives with different alkyl chain lengths (C15–C18) were prepared, and their 2D structures were studied by STM at the HOPG/TCB interface. Due to the presence of the methoxy group, the **CR** compounds showed identical linear structures with interdigitated alkyl chains, regardless of the alkyl chain length. In the case of **TC** compounds, **TC15** showed an interdigitated Z-like configuration, whereas **TC16–18** compounds showed a V-like conformation, in which the alkyl chains adopted a tail-to-tail arrangement without interdigitation. When the number of methoxy or alkoxy groups increased, the 2D self-assembled structure was dominated by the molecule–substrate interaction rather than intermolecular interaction between the alkyl chains of adsorbed molecules. Therefore, no odd–even effect was observed in the 2D structures of **CR** and **TC** compounds.

However, the 2D structures of **BC** compounds were alternately modulated, depending on the alkyl chain length. The **BC** compounds with odd carbon numbers in alkyl chains exhibited stair-like structures. Moreover, some of the alkyl chains dangled into the liquid phase due to space limitation. **BC** compounds with even carbon numbers showed linear arrangements with interdigitated alkyl chains. The absence of alkoxy groups at the 3-positions of the derivatives made the intermolecular interactions of the alkyl chains more effective, resulting in the odd–even effect.

The present results demonstrate that tuning the balance

between in-plane intermolecular and molecule–substrate interactions is an efficient strategy to modulate the appearance of the odd–even effects, which contribute to the control of the 2D molecular patterns at the solid/liquid interface. We are currently investigating molecular network formation using bio-based materials including curcumin derivatives, which will be reported in due course.

Conflicts of interest

There are no conflicts to declare.

Acknowledgements

This work was partly supported by JST SPRING (JPMJSP2124), and a grant from the Iketani Science and Technology Foundation (0331054-A).

Notes and references

- (a) J. P. Rabe and S. Buchholz, *Science*, 1991, **253**, 424–427. (b) S. De Feyter and F. C. De Schryver, *Chem. Soc. Rev.*, 2003, **32**, 139–150. (c) D. L. Allara, *Nature*, 2005, **437**, 638–639. (d) C. B. Tang, E. M. Lennon, G. H. Fredrickson, E. J. Kramer, and C. J. Hawker, *Science*, 2008, **322**, 429–432. (e) C. Tang, S.-M. Hur, B. C. Stahl, K. Sivanandan, M. Dimitriou, E. Pressly, G. H. Fredrickson, E. J. Kramer, and C. J. Hawker, *Macromolecules*, 2010, **43**, 2880–2889.
- (a) Y. Kikkawa, E. Koyama, S. Tsuzuki, K. Fujiwara, and M. Kanetsato, *Langmuir*, 2010, **26**, 3376–3381. (b) N. Li, Y. Y. Liu, Y. Li, J. B. Zhuang, R. R. Cui, Q. Gong, N. Zhao, and B. Z. Tang, *ACS Appl. Mater. Interfaces*, 2018, **10**, 24249–24257. (c) I. Matsumoto, R. Sekiya, and T. Haino, *Angew. Chem., Int. Ed.*, 2021, **60**, 12706–12711.
- (a) J. Otsuki, *Coord. Chem. Rev.* 2010, **254**, 2311–2341. (b) Y. F. Geng, P. Li, J. Z. Li, X. M. Zhang, Q. D. Zeng, and C. Wang, *Coord. Chem. Rev.*, 2017, **337**, 145–177. (c) Y. F. Geng, P. Li, J. Z. Li, X. M. Zhang, Q. D. Zeng, and C. Wang, *Coord. Chem. Rev.*, 2017, **337**, 145–177. (d) X. Sun, X. Yao, F. Lafolet, G. Lemerrier, and J.-C. Lacroix, *J. Phys. Chem. Lett.*, 2019, **10**, 4164–4169. (e) X. Sun, X. Yao, G. Trippé-Allard, and J.-C. Lacroix, *J. Phys. Chem. C*, 2021, **125**, 957–963. (f) Y. Kikkawa, M. Nagasaki, S. Tsuzuki, T. N. J. Fouquet, S. Nakamura, Y. Takenaka, Y. Norikane, and K. Hiratani, *Chem. Comm.*, 2022, **58**, 1752–1755.
- (a) D. González-Rodríguez and A. P. H. J. Schenning, *Chem. Mater.*, 2011, **23**, 310–325. (b) K. Miao, Y. Hu, B. Zha, L. Xu, X. Miao, and W. Deng, *J. Phys. Chem. C*, 2016, **120**, 14187–14197. (c) Y. Wu, J. Li, Y. Yuan, M. Dong, B. Zha, X. Miao, Y. Hu, and W. Deng, *Phys. Chem. Chem. Phys.*, 2017, **19**, 3143–3150. (d) C. Zhang, F. Wang, R. S. Patil, C. L. Barnes, T. Li, and J. L. Atwood, *Chem. - Eur. J.*, 2018, **24**, 14335–14340. (e) N. Nishitani, T. Hirose, and K. Matsuda, *Chem. Lett.*, 2019, **48**, 253–256.
- (a) H. L. Nguyen, P. N. Horton, M. B. Hursthouse, A. C. Legon, and D. W. Bruce, *J. Am. Chem. Soc.*, 2004, **126**, 16–17. (b) F. Wang, N. Ma, Q. Chen, W. Wang, and L. Wang, *Langmuir*, 2007, **23**, 9540–9542. (c) F. Silly, *J. Phys. Chem. C*, 2013, **117**, 20244–20249. (d)

- M. Dong, J. Wu, X. Miao, J. Li, and W. Deng, *J. Phys. Chem. C*, 2019, **123**, 26191–26200. (e) J. Teyssandier, K. S. Mali, and S. De Feyter, *ChemistryOpen*, 2020, **9**, 225–241. (f) Y. Kikkawa, M. Nagasaki, E. Koyama, S. Ito, and S. Tsuzuki, *Phys. Chem. Chem. Phys.*, 2022, **24**, 17088–17097.
6. (a) D. M. Cyr, B. Venkataraman, and G. W. Flynn, *Chem. Mater.*, 1996, **8**, 1600–1615. (b) S. De Feyter, A. Gesquière, M. M. Abdel-Mottaleb, P. C. M. Grim, F. C. De Schryver, C. Meiners, M. Sieffert, S. Valiyaveetil, and K. Müllen, *Acc. Chem. Res.*, 2000, **33**, 520–531. (c) S. De Feyter and F. C. De Schryver, *J. Phys. Chem. B*, 2005, **109**, 4290–4302. (d) W. Mamdouh, H. Uji-I, J. S. Ladislaw, A. E. Dulcey, V. Percec, F. C. De Schryver, and S. De Feyter, *J. Am. Chem. Soc.*, 2006, **128**, 317–325.
7. (a) F. Tao and S. L. Bernasek, *Chem. Rev.*, 2007, **107**, 1408–1453. (b) Z. Ma, Y. Y. Wang, P. Wang, W. Huang, Y. B. Li, S. B. Lei, Y. L. Yang, X. L. Fan, and C. Wang, *ACS Nano*, 2007, **1**, 160–167. (c) Q. Chen, H. J. Yan, C. J. Yan, G. B. Pan, L. J. Wan, G. Y. Wen, and D. Q. Zhang, *Surf. Sci.*, 2008, **602**, 1256–1266. (d) H. Xu, A. Minoia, Ž. Tomović, R. Lazzaroni, E. W. Meijer, A. P. H. J. Schenning, and S. De Feyter, *ACS Nano*, 2009, **3**, 1016–1024. (e) Y. Hu, K. Miao, B. Zha, L. Xu, X. Miao, and W. Deng, *Phys. Chem. Chem. Phys.*, 2016, **18**, 624–634.
8. (a) E. Ghijsens, O. Ivashenko, K. Tahara, H. Yamaga, S. Itano, T. Balandina, Y. Tobe, and S. De Feyter, *ACS Nano*, 2013, **7**, 8031–8042. (b) X. Wang, G. He, Y. Li, Z. Kuang, Q. Guo, J.-L. Wang, J. Pei, and A. Xia, *J. Phys. Chem. C*, 2017, **121**, 7659–7666. (c) Y. Kikkawa, S. Tsuzuki, K. Taguchi, A. Kashiwada, and K. Hiratani, *Phys. Chem. Chem. Phys.*, 2017, **19**, 13579–13584. (d) A. T. Röscher, R. Reynaerts, B. A. G. Lamers, K. S. Mali, S. De Feyter, A. R. A. Palmans, and E. W. Meijer, *Chem. Mater.*, 2021, **33**, 8800–8811.
9. (a) K. Omori, Y. Kikkawa, M. Kanesato, and K. Hiratani, *Chem. Comm.*, 2010, **46**, 8008–8010. (b) Y. Kikkawa, E. Koyama, S. Tsuzuki, K. Fujiwara, and M. Kanesato, *Langmuir*, 2010, **26**, 3376–3381. (c) H. Cao, K. Tahara, S. Itano, Y. Tobe, and S. De Feyter, *J. Phys. Chem. C*, 2017, **121**, 10430–10438. (d) Y. Hu, S.-L. Lee, and W. Deng, *Langmuir*, 2022, **38**, 1757–1765. (e) Y. Wang, H. Gao, M. Ke, X. Zeng, X. Miao, X. Cheng, and W. Deng, *Langmuir*, 2022, **38**, 7005–7012.
10. (a) T. Garrison, A. Murawski, and R. Quirino, *Polymers*, 2016, **8**, 262. (b) M. T. Chorsi, E. J. Curry, H. T. Chorsi, R. Das, J. Baroody, P. K. Purohit, H. Ilies, and T. D. Nguyen, *Adv. Mater.*, 2019, **31**, 1802084. (c) F. Hartmann, M. Baumgartner, and M. Kaltenbrunner, *Adv. Mater.*, 2021, **33**, 2004413.
11. (a) T. Garrison, A. Murawski and R. Quirino, *Polymers*, 2016, **8**, 262. (b) F. Jiao, Y. Chen, H. Jin, P. He, C.-L. Chen, and J. J. De Yoreo, *Adv. Funct. Mater.*, 2016, **26**, 8960–8967. (c) H. Jin, F. Jiao, M. D. Daily, Y. Chen, F. Yan, Y.-H. Ding, X. Zhang, E. J. Robertson, M. D. Baer, and C.-L. Chen, *Nat. Commun.*, 2016, **7**, 12252. (d) M. Zhu, J. Liu, L. Gan, and M. Long, *Eur. Polym. J.*, 2020, **129**, 109651.
12. (a) S. Wanninger, V. Lorenz, A. Subhan, and F. T. Edelmann, *Chem. Soc. Rev.*, 2015, **44**, 4986–5002. (b) M. Prohl, U. S. Schubert, W. Weigand, and M. Gottschaldt, *Coord. Chem. Rev.*, 2016, **307**, 32–41. (c) Y. Panahi, O. Fazlollahzadeh, S. L. Atkin, M. Majeed, A. E. Butler, T. P. Johnston, and A. Sahebkar, *J. Cell. Physiol.*, 2019, **234**, 1165–1178.
13. M. Lozada-García, R. Enríquez, T. Ramírez-Apán, A. Nieto-Camacho, J. Palacios-Espinosa, Z. Custodio-Galván, O. Soria-Arteche, and J. Pérez-Villanueva, *Molecules*, 2017, **22**, 633.
14. Gaussian 16, Revision C.01, M. J. Frisch, G. W. Trucks, H. B. Schlegel, G. E. Scuseria, M. A. Robb, J. R. Cheeseman, G. Scalmani, V. Barone, G. A. Petersson, H. Nakatsuji, X. Li, M. Caricato, A. V. Marenich, J. Bloino, B. G. Janesko, R. Gomperts, B. Mennucci, H. P. Hratchian, J. V. Ortiz, A. F. Izmaylov, J. L. Sonnenberg, D. Williams-Young, F. Ding, F. Lipparini, F. Egidi, J. Goings, B. Peng, A. Petrone, T. Henderson, D. Ranasinghe, V. G. Zakrzewski, J. Gao, N. Rega, G. Zheng, W. Liang, M. Hada, M. Ehara, K. Toyota, R. Fukuda, J. Hasegawa, M. Ishida, T. Nakajima, Y. Honda, O. Kitao, H. Nakai, T. Vreven, K. Throssell, J. A. Montgomery, Jr., J. E. Peralta, F. Ogliaro, M. J. Bearpark, J. J. Heyd, E. N. Brothers, K. N. Kudin, V. N. Staroverov, T. A. Keith, R. Kobayashi, J. Normand, K. Raghavachari, A. P. Rendell, J. C. Burant, S. S. Iyengar, J. Tomasi, M. Cossi, J. M. Millam, M. Klene, C. Adamo, R. Cammi, J. W. Ochterski, R. L. Martin, K. Morokuma, O. Farkas, J. B. Foresman, and D. J. Fox, Gaussian, Inc., Wallingford CT, 2016. A. D.
15. A. D. Becke, *J. Chem. Phys.*, 1993, **98**, 5648–5652.
16. S. Grimme, J. Antony, S. Ehrlich and H. Krieg, *J. Chem. Phys.*, 2010, **132**, 154104.
17. S. F. Boys and F. Bernardi, *Mol. Phys.*, 1970, **19**, 553–566.
18. S. Tsuzuki, K. Honda, T. Uchamaru, and M. Mikami, *J. Phys. Chem. A*, 2004, **108**, 10311–10316.
19. K. Tahara, R. Nakayama, M. Maeda, S. De Feyter, and Y. Tobe, *J. Phys. Chem. C*, 2019, **123**, 27020–27029.
20. S. Tsuzuki, H. Houjou, Y. Nagawa, and K. Hiratani, *J. Chem. Soc., Perkin Trans. 2*, 2002, 1271–1273.